



CHORUS

This is the accepted manuscript made available via CHORUS. The article has been published as:

Phase conversion dissipation in multicomponent compact stars

Mark G. Alford, Sophia Han (✉), and Kai Schwenzer

Phys. Rev. C **91**, 055804 — Published 11 May 2015

DOI: [10.1103/PhysRevC.91.055804](https://doi.org/10.1103/PhysRevC.91.055804)

Phase conversion dissipation in multi-component compact stars

Mark G. Alford, Sophia Han (韩君), Kai Schwenzer

Physics Department, Washington University, St. Louis, MO 63130, USA

(Dated: 30 Jan 2015)

We propose a mechanism for the damping of density oscillations in multi-component compact stars. The mechanism is the periodic conversion between different phases, i.e. the movement of the interface between them, induced by pressure oscillations in the star. The damping grows nonlinearly with the amplitude of the oscillation. We study in detail the case of r-modes in a hybrid star with a sharp interface, and we find that this mechanism is powerful enough to saturate the r-mode at very low saturation amplitude, of order 10^{-10} , and is therefore likely to be the dominant r-mode saturation mechanism in hybrid stars with a sharp interface.

PACS numbers: 25.75.Nq, 26.60.-c, 97.60.Jd,

I. INTRODUCTION

The damping of mechanical oscillations of compact stars is a promising signature of the phases of dense matter in their interior. The damping of density perturbations, described locally by the bulk viscosity, is particularly important since it has been shown to vary greatly between different phases [1–14]. In addition to the damping properties of bulk phases, the boundary between different phases can also be relevant for dissipation. A well-known example is Ekman layer damping due to shear forces at the boundary between a fluid and a solid phase [15]. Here we propose a dissipation mechanism that stems from the fact that pressure oscillations can cause the interface between two phases to move back and forth, as the two phases are periodically converted into each other. If the finite rate of this conversion produces a phase lag between the pressure oscillation and the position of the interface, energy will be dissipated in each cycle. We study the resultant damping for the case of a hybrid star with a sharp interface between the quark core and the hadronic mantle, where the dissipation is due to quark-hadron burning at the interface. However, the mechanism is generic and could be relevant for any star with an internal interface between phases of different energy density.

Unstable global oscillation modes [16] are of particular interest since they arise spontaneously and grow until stopped by some saturation (nonlinear damping) mechanism. For neutron stars, the most important example is r-modes [17, 18] since they are unstable in typical millisecond pulsars unless sufficient damping is present. Several mechanisms for the saturation of the growth of unstable r-modes have been proposed [19–24]. Although bulk viscosity has a nonlinear “suprathermal” regime [3, 25, 26], it has been found that this becomes relevant only at very high amplitudes, and is probably pre-empted by some other stronger mechanism [22]. In this paper we show that dissipation due to hadron-quark burning could well be the dominant r-mode saturation mechanism in hybrid stars. The dissipation is vanishingly small at infinitesimal amplitude, but becomes very strong as the amplitude increases. (For similar behavior

in a different context see [24]). This strong dissipation saturates unstable r-modes in compact stars with a sufficiently large core at amplitudes that are orders of magnitude below those provided by any other known saturation mechanism. We give a simple analytic prediction for the saturation amplitude, and find that it can be as low as $\alpha_{\text{sat}} \lesssim 10^{-10}$ for conditions present in observed pulsars.

II. SCHEMATIC MODEL FOR THE DISSIPATION DUE TO PHASE TRANSFORMATION

A. Two phases in a cylinder

As a step towards an analysis of the dissipation due to phase conversion in an inhomogeneous multi-component star, we now construct a simplified version of the interface between different layers in a gravitationally bound system. We will calculate the energy dissipated in this system when it is subjected to periodic compression and rarefaction.

Our toy system involves two incompressible phases, characterized by different densities of a conserved particle species. We assume there is a first-order pressure-induced phase transition, so the phases are separated by a sharp interface (“the phase boundary”) which, in long-term equilibrium, is at the critical pressure p_{crit} , and that there are processes that can convert each phase into the other at some finite rate. We consider a cylinder containing both phases in a homogeneous (Newtonian) gravitational field, with a piston which can be moved parallel to the direction of the field (Fig. 1). The high-density phase is deeper in the gravitational potential than the low-density phase. The field produces a pressure gradient in the cylinder, which can be shifted by moving the piston. This will cause the equilibrium position of the interface to shift, but, crucially, depending on the speed of the conversion process, it may take some time for the interface to move to its new equilibrium position. This causes the response of the system (its volume or density) to lag behind the externally applied force, resulting in dissipation. To calculate the energy dissipated per cycle,

we simply calculate the net $p dV$ work done by the piston in one cycle.

We will assume that the equation of state of the two phases is linear,

$$p(\mu) = \begin{cases} \mu n_L - \varepsilon_L & \text{(low density phase)} \\ \mu n_H - \varepsilon_H & \text{(high density phase)} \end{cases}, \quad (1)$$

where μ is the chemical potential for the conserved particle number, and the two incompressible phases have fixed particle number densities n_L and n_H , and fixed energy densities ε_L and ε_H . Later we will use the fact that this is a valid approximation for any equation of state, as long as the pressure oscillations are small enough.

In a Newtonian gravitational field the pressure is a function of x determined by

$$\frac{dp}{dx} = -g\varepsilon, \quad (2)$$

where g is the gravitational acceleration, assumed to be independent of x . Eq. (2) has a simple solution where the pressure varies linearly with x , with a fixed gradient $g\varepsilon$ in each phase (see Fig. 2)

$$p(x) = \begin{cases} p_b - g\varepsilon_H(x - x_b) & x < x_b \\ p_b - g\varepsilon_L(x - x_b) & x \geq x_b \end{cases}, \quad (3)$$

where x_b is the position of the interface between the two phases (“the boundary”) and p_b is the pressure at the boundary. In long-term equilibrium, the boundary settles at its “ideal” position, where p_b is p_{crit} (see below).

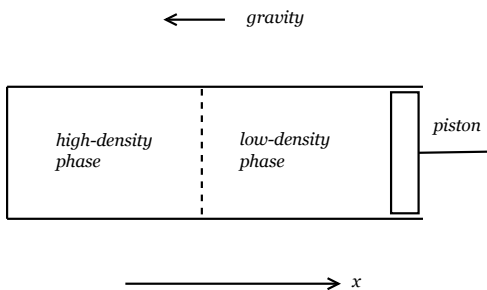


FIG. 1: Toy model: two incompressible phases in a cylinder with piston, in a gravitational field. An oscillation of the external pressure on the piston leads to interconversion of the two phases, and hence movement of the piston.

B. External pressure oscillation

Assume that the external pressure on the piston varies periodically. When the pressure is high, part of the low-density phase is driven to a pressure above p_{crit} and starts

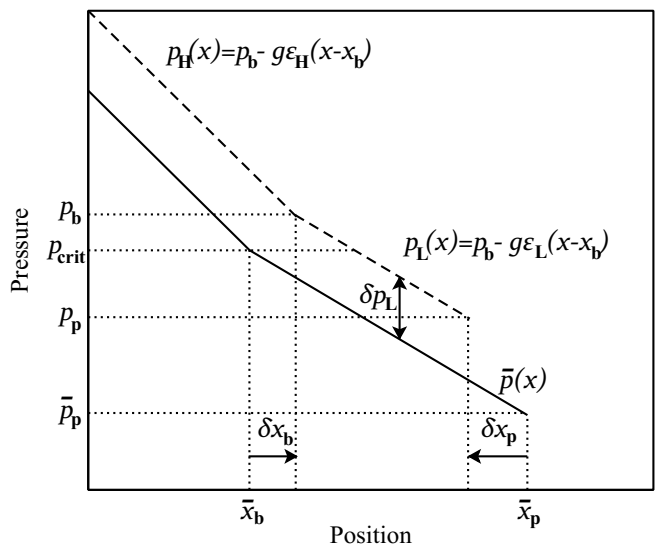


FIG. 2: Pressure gradients in the cylinder of Fig. 1. Solid line $\bar{p}(x)$ is the pressure profile in long-term equilibrium. Dashed line is a snapshot of the system at a moment when the piston has moved inward a distance δx_p , the pressure everywhere has risen, and the phase boundary has moved out a distance δx_b as the low density phase in part of the region with $p > p_{\text{crit}}$ has converted to the high-density phase.

to convert into the high density phase, and vice versa during rarefaction. The pressure at any given location and the position of the phase boundary therefore vary in time

$$p(x, t) = \bar{p}(x) + \delta p(x, t), \quad (4)$$

$$x_b(t) = \bar{x}_b + \delta x_b(t), \quad (5)$$

where \bar{x}_b is the equilibrium position of the boundary and $\bar{p}(x)$ is the pressure profile in long-term equilibrium. The position of the boundary at a given moment depends on the previous compression history and the phase conversion rate, and we expect that, because of the finite rate of conversion between the two phases, the oscillation of the boundary can be out of phase with the oscillation of the pressure, and this will lead to dissipation via net $p dV$ work being done in each cycle.

To calculate the dissipation, we need to relate the movement of the boundary to the applied pressure oscillation. We assume that the pressure in the low density phase oscillates harmonically with amplitude Δp_L and frequency ω , so $\delta p_L(t) = \Delta p_L \sin(\omega t)$.

In equilibrium, the piston is at \bar{x}_p with pressure \bar{p}_p . As part of the pressure oscillation the piston moves

$$x_p(t) = \bar{x}_p + \delta x_p(t), \quad (6)$$

and the pressure at the piston is

$$p_p(t) = \bar{p}_p - g\varepsilon_L \delta x_p(t) + \Delta p_L \sin(\omega t) \quad (7)$$

The movement of the piston and the movement of the phase boundary are connected by particle number conservation inside the cylinder. The total particle number

is $N_{\text{tot}} = (x_b(t)n_H + (x_p(t) - x_b(t))n_L)S$ where S is the cross sectional area. Particle number conservation $\delta N_{\text{tot}} = 0$ gives

$$x_p(t) = \bar{x}_p + \left(1 - \frac{n_H}{n_L}\right) \delta x_b(t). \quad (8)$$

We can now express the $p dV$ work done by the piston in one cycle in terms of the movement of the boundary δx_b induced by the pressure oscillation. In later sections we will study how the boundary moves, expressing it as a function of the speed of the phase conversion process. First, however, we define a useful concept, the ‘‘ideal boundary’’.

C. Ideal position of the phase boundary

In discussing the motion of the boundary it is convenient to define an ‘‘ideal position’’ of the boundary, x_{ib} . Since we are assuming that an external force imposes a specified time-dependence of the pressure in the low-density phase, it is natural to define the ideal boundary at time t to be the position the boundary would reach if we held δp_L fixed at its current value and waited for phase conversion processes to equilibrate. Thus $x_{\text{ib}}(t)$ is the solution of $p_L(x_{\text{ib}}, t) = p_{\text{crit}}$. Unlike the actual boundary, the ideal boundary is determined simply by the instantaneous value of the applied pressure, with no dependence on previous history or conversion rate. The position of the ideal boundary therefore oscillates in phase with the pressure,

$$\delta x_{\text{ib}}(t) = \Delta x_{\text{ib}} \sin(\omega t), \quad \Delta x_{\text{ib}} = \frac{\Delta p_L}{g \varepsilon_L} \quad (9)$$

and its velocity is 90° out of phase with its position

$$v_{\text{ib}}(t) = v_{\text{ib}}^{\text{max}} \cos(\omega t), \quad v_{\text{ib}}^{\text{max}} = \omega \Delta x_{\text{ib}} = \frac{\omega \Delta p_L}{g \varepsilon_L}. \quad (10)$$

For a harmonic pressure oscillation in the low-density phase the ideal boundary moves harmonically. Note however, that because of the discontinuity in energy density on the phase boundary, the pressure oscillation cannot be simultaneously harmonic in both phases. It is also worth noting that according to our definition $x_{\text{ib}}(t)$ is not in general the place in the cylinder where the pressure at time t is p_{crit} : these locations only coincide if the real phase boundary occurs where the pressure is above p_{crit} .

D. Energy dissipation in one cycle

The net $p dV$ work done by the piston in one cycle ($0 \leq t < \tau$, $\tau = 2\pi/\omega$) is

$$W = -S \int_0^\tau p_p(t) \frac{dx_p(t)}{dt} dt \quad (11)$$

where p_p is the pressure at the location of the piston, which is determined by the applied oscillation of the piston, and x_p is the position of the piston. The piston’s position depends on the movement of the boundary $\delta x_b(t)$ (8), so from Eq. (11) the energy dissipation in one cycle is

$$W = S \left(\frac{n_H}{n_L} - 1 \right) \left(\int_0^\tau \bar{p}_p \frac{d\delta x_b(t)}{dt} dt + \int_0^\tau \Delta p_L \sin(\omega t) \frac{d\delta x_b(t)}{dt} dt \right) \quad (12)$$

The movement of the boundary is constrained by the detailed physics of the conversion process, which determines how fast it can move at any given moment. For quark/hadron conversion we will see that it obeys a differential equation which expresses the fact that the boundary’s maximum velocity depends on how far out of equilibrium the boundary is, and whether it needs to move inward or outward to reach equilibrium. In effect, the real boundary is always chasing the ideal boundary (which is its long run equilibrium position), while the ideal boundary is a moving target, its sinusoidal movement linearly related to the applied pressure oscillation, see Eqs. (7) and (9).

In Eq. (12) we see that the dissipation vanishes if the two phases have equal densities, since then the movement of the phase boundary does not change the volume of the system, so there is no associated $p dV$ work.

To derive the dissipation we assumed that the pressure oscillation in the low density phase is harmonic. Had we instead assumed that the pressure oscillation in the high density phase is harmonic, then the energy dissipation would be slightly bigger, with a difference $\Delta W/W \simeq \Delta \varepsilon/\varepsilon_L$, where $\Delta \varepsilon$ is the energy density discontinuity at the interface.

III. R-MODE DAMPING

We can now calculate the damping of a global oscillation mode in a hybrid star resulting from the phase conversion mechanism. A comprehensive analysis of this problem requires the detailed density oscillation of the global mode in a star with multiple components separated by density discontinuities due to first order phase transitions. So far the profiles for global oscillation modes have not been obtained for such a realistic model of a compact star. We will therefore estimate the dissipation from a piecewise model for the mode profile, using the known form for a homogeneous star on either side of the phase boundary. We estimate the error due to this simplified procedure below. Although the amplitude of the mode’s density and pressure oscillation varies from place to place in the star, the simple model sketched in Sec. II then applies locally for sufficiently small volume elements containing the interface between the two phases and the entire range over which it moves in response to the oscillation.

Here we study the case of r-modes because they are unstable and a sufficiently powerful damping mechanism is required to ensure that they saturate at a low enough amplitude so that they do not spin down the fast rotating compact stars that we observe. The energy density fluctuation for an $m=2$ r-mode to leading order in the mode amplitude α is [27]

$$\frac{\delta\varepsilon}{\bar{\varepsilon}} = \sqrt{\frac{8}{189}} \alpha A R^2 \Omega^2 \left(\frac{r}{R}\right)^3 \operatorname{Re} [Y_3^2(\theta, \phi) e^{i\omega t}] \quad (13)$$

where $\delta\varepsilon = \varepsilon - \bar{\varepsilon}$, $Y_3^2(\theta, \phi) = \frac{1}{4} \sqrt{\frac{105}{2\pi}} e^{2i\phi} \sin^2\theta \cos\theta$, and A is the inverse speed of sound squared

$$A \equiv \frac{\partial\varepsilon}{\partial p} \quad (14)$$

evaluated at equilibrium. R is the radius of the star, Ω the rotational frequency of the star, and ω is the r-mode frequency $\omega = \frac{2}{3}\Omega$.

The r-mode involves flows that are dominantly angular rather than radial. At any moment there is higher pressure in some regions of solid angle in the star, and lower pressure in other regions. This means that globally the fraction of high or low pressure phase does not change much over time. However, an r-mode will still lead to conversion between the phases, since the low and high pressure regions are kilometers apart, so the gradients of pressure and density in the angular directions are extremely small, and in an oscillation at kHz frequencies there is not enough time for any response other than local movement of the boundary in the radial direction. Therefore particle transformation is required in far-separated areas despite the approximate global conservation of the amount of each of the two forms of matter. The simple cylinder and piston model of Sec. II is a valid approximation for a small volume element that straddles the interface between the two phases. To use the results from Sec. II we simply need to use the appropriate expression for the local gravitational acceleration g . The general relativistic generalization of the Newtonian hydrostatic equation is the Oppenheimer-Volkoff (OV) equation [28]

$$\begin{aligned} \frac{dp}{dr} &= -g_{\text{eff}}(r)\epsilon(r) \\ g_{\text{eff}}(r) &= \frac{GM}{r^2} \left(1 + \frac{p}{\epsilon}\right) \left(1 + \frac{4\pi p r^3}{M}\right) \left(1 - \frac{2M}{r}\right)^{-1} \end{aligned} \quad (15)$$

where p , ϵ and M , given by $(dM)/(dr) = 4\pi r^2 \epsilon$, depending on the radial position. The effective gravitational acceleration g_{eff} contains general relativistic corrections to its Newtonian value M/r^2 .

A. Movement of the ideal boundary

We will now calculate the dissipation of the energy of an r-mode in a star with a high density core surrounded by a low density mantle. (In the next section we

will look at the case where the phases are quark matter and hadronic matter.) We are interested in situations where phase conversion dissipation becomes important in r-mode oscillations when their amplitude is still fairly low (we will see in Sec. IVD that this may indeed happen), so we will assume $\delta p \ll \bar{p}$ in the region near the boundary. Therefore, we only need the EoS in a narrow pressure range around the critical pressure. The EoS can be expanded to linear order analogous to Eq. (1) so the pressure oscillation is given by

$$\delta p = \frac{\bar{\varepsilon}}{A} \frac{\delta\varepsilon}{\bar{\varepsilon}}. \quad (16)$$

When $\delta\varepsilon > 0$, according to Eq. (13)–(16) the r-mode pressure oscillation in the low density phase is

$$\delta p_L(r, \theta, \phi, t) = \bar{\varepsilon}_L(r) C(r) \alpha \sin^2\theta \cos\theta \cos(2\phi + \omega t) \quad (17)$$

where

$$C(r) \equiv \sqrt{\frac{105}{756\pi}} \Omega^2 \frac{r^3}{R} \quad (18)$$

The ideal (i.e. long-run equilibrium at given pressure) position of the boundary R_{ib} , analogous to x_{ib} in Sec. II, is determined by the r-mode pressure oscillation in the low-density phase, and therefore depends on the angular co-ordinates. If we write $R_{\text{ib}} = \bar{R}_b + \delta R_{\text{ib}}$, where \bar{R}_b is the equilibrium position of the phase boundary with no pressure oscillation, then from (15) and (17)

$$\delta R_{\text{ib}}(t) = \frac{\delta p_L}{dp/dr(\bar{R}_b)} = \frac{\alpha C_b}{g_b} \sin^2\theta \cos\theta \cos(2\phi + \omega t) \quad (19)$$

where

$$\begin{aligned} g_b &\equiv g_{\text{eff}}(\bar{R}_b) \\ C_b &\equiv C(\bar{R}_b) = \sqrt{\frac{105}{756\pi}} \Omega^2 \frac{\bar{R}_b^3}{R}. \end{aligned} \quad (20)$$

and $g_{\text{eff}}(\bar{R}_b)$ is the effective gravitational acceleration at \bar{R}_b evaluated in the low-density phase.

The oscillation amplitude of the ideal boundary position, as a function of latitude θ in the star, is

$$|\delta R_{\text{ib}}| = \frac{C_b \alpha}{g_b} |\sin^2\theta \cos\theta| \quad (21)$$

and the maximum value of the velocity of the ideal boundary $v_{\text{ib}}^{\text{max}}$ is

$$v_{\text{ib}}^{\text{max}} = \frac{C_b \alpha \omega}{g_b} |\sin^2\theta \cos\theta| \quad (22)$$

B. R-mode energy dissipation

We now calculate $dW(\theta, \phi)$, the energy dissipated during one oscillation cycle in a radially oriented cylinder

straddling the phase boundary, with an infinitesimal base area located at a given spherical angle. Integrating this result over solid angle will give the total dissipation of the r-mode. Using Eqs. (12) and (19),

$$dW(\theta, \phi) = dS \left(\frac{n_H}{n_L} - 1 \right) \Delta p_L \int_0^\tau \cos(2\phi + \omega t) \frac{d\delta R_b(t)}{dt} dt \quad (23)$$

where $\Delta p_L = g_b \varepsilon_{\text{crit}}^L |\delta R_{\text{ib}}|$, and from Eq. (21)

$$\Delta p_L = \varepsilon_{\text{crit}}^L C_b \alpha |\sin^2 \theta \cos \theta| \quad (24)$$

and $dS = \bar{R}_b^2 \sin \theta d\theta d\phi$. As discussed earlier, these estimates are based on an approximate r-mode profile. To estimate the uncertainty due to this simplification we compare two idealized cases, where the pressure oscillation is harmonic in the low density phase, and where it is harmonic in the high-density phase. As discussed below Eq. (12) the difference for an infinitesimal volume element is of order $\Delta W/W \simeq \Delta \varepsilon/\varepsilon_L$ which directly gives an estimate for the uncertainty of the dissipation in the case of global r-modes. Typical density steps at first order transitions in a compact star are less than a factor of two, but due to the simplified model assumptions we make here our results should anyway be viewed as order of magnitude estimates.

IV. HADRON/QUARK CONVERSION IN A HYBRID STAR

The damping mechanism that we have analyzed above is generic, and will operate in any situation where there are two phases with a sharp interface. However, the amount of damping depends crucially on how the interface between the two phases moves via conversion of one phase into the other. To explore a realistic case, we will now estimate the boundary velocity for an interface between strange quark matter and nuclear matter in a hybrid star, and obtain an estimate of the resultant r-mode saturation amplitude in this scenario.

It is worth mentioning that the scenario depicted here of a smooth and steadily moving phase boundary might be disturbed by instabilities that lead to a turbulent burning front. In the conversion of a neutron star to a quark star, this instability occurs and may lead to a detonation [29] or a deflagration [30–32]. That full conversion process occurs when quark matter is the preferred state all the way down to zero pressure (the “strange matter hypothesis”). In our situation, however, the conversion is much slower: we study the case where conversion of hadronic matter to quark matter occurs only at a high critical pressure. The movement of the phase boundary in our case is driven by a small deviation from equilibrium, induced by oscillations. We defer the study of turbulent instabilities in this context to future work.

We will use the calculational techniques developed by Olinto [33] to study the movement of the phase boundary in the strange matter hypothesis scenario, but we are

interested in conversion of quark matter to nuclear matter as well as nuclear matter to quark matter, since both processes occur as our burning front moves inwards and outwards periodically in response to an oscillation in the pressure.

A. Pressure and chemical potential at the interface

In equilibrium, both pressure and baryon chemical potential are continuous across the phase boundary between nuclear and quark matter, and their values at the boundary are the critical values at which the phase transition occurs ($p = p_{\text{crit}}, \mu_B = \mu_B^{\text{crit}}$). When the system is driven out of equilibrium by global pressure oscillations, the phase boundary may temporarily be at a different pressure because the conversion between nuclear and quark matter has a limited rate. The boundary is then out of chemical equilibrium, and the baryon chemical potential is no longer continuous at the boundary because baryon number cannot flow freely through the boundary. On the timescale of chemical equilibration the pressure is still continuous because it equilibrates at the speed of sound which is of order c . The burning front will move as the phase with higher baryon chemical potential converts into the phase with lower baryon chemical potential. The situation is illustrated in Fig. 3. If the pressure at the boundary is above the critical value ($p_b = p_1 > p_{\text{crit}}$), the baryon number chemical potential in quark matter is lower ($\mu_1^Q < \mu_1^N$). Nuclear matter (NM) is then converted into quark matter (QM) and the front moves outwards. If the pressure at the boundary is below the critical value ($p_b = p_2 < p_{\text{crit}}$) the front moves in the opposite direction converting quark matter back into nuclear matter.

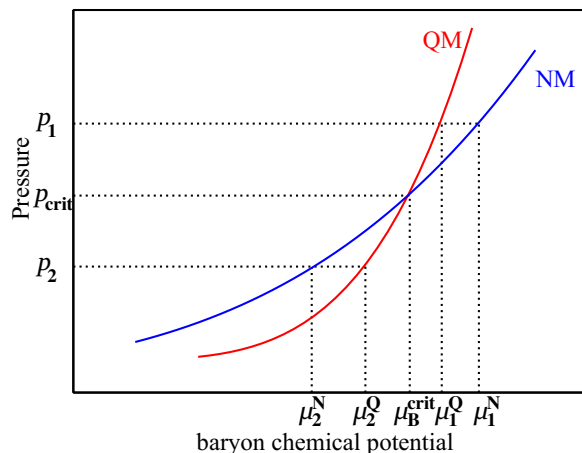


FIG. 3: (Color online) Schematic plot of the pressure as a function of baryon chemical potential in beta-equilibrated ($\mu_K = 0$) nuclear matter and quark matter. At a given pressure, the phase with lower μ_B is thermodynamically favored.

As we will see below, when the boundary is out of

chemical equilibrium, and moving to reestablish that equilibrium, it has around it a $\text{NM} \rightleftharpoons \text{QM}$ conversion region, where the matter is out of beta equilibrium.

The chemical equilibration of quark matter can proceed via the nonleptonic channel $u + s \leftrightarrow d + u$ and also the leptonic Urca channel $d \rightarrow u + e^- + \bar{\nu}$ and $u + e^- \rightarrow d + \nu$. Following Ref. [33], we neglect the Urca channel here for simplicity, but we discuss its potential impact in Sec. V. Nonleptonic beta-equilibration processes are driven by the chemical potential μ_K , which couples to the imbalance between strange and down quarks; μ_K is zero in beta equilibrated matter, but not in the conversion region,

$$\begin{aligned} \mu_K &\equiv \mu_d - \mu_s, \\ n_K &= \frac{1}{2}(n_d - n_s). \end{aligned} \quad (25)$$

In the following sections we discuss how μ_K and μ_B vary in the conversion region when the front is moving, in order to estimate the speed of the boundary in two half cycles of oscillation, which determines the energy dissipation over the complete period.

B. Conversion of nuclear matter into quark matter

To estimate the front speed in the $\text{NM} \rightarrow \text{QM}$ transition when $p_b = p_1 > p_{\text{crit}}$, we use the one-dimensional steady-state approximation used by Olinto [33] to study the irreversible conversion of nuclear matter to strange matter in the scenario where strange quark matter is stable at zero pressure. In our scenario there is a critical pressure at which the transition occurs, with conversion going in either direction depending on the history of the system, but Olinto's approach is still applicable. The analysis is conveniently performed in the rest frame of the boundary, where the boundary is at $x = 0$, neutron matter is at $x < 0$ and strange quark matter at $x > 0$. The transformation of neutron matter into strange quark matter requires considerable strangeness production, which can only be accomplished by flavor-changing weak interactions. The slow rate of weak interactions means that at the front nuclear matter is converted in to some form of non-beta-equilibrated quark matter (with $\mu_K \neq 0$). In the conversion region behind the front there are flavor-changing non-leptonic interactions and strangeness diffusion. The weak interactions create strangeness and allow μ_K to return to zero over a distance scale of order $(D_Q \tau_Q)^{1/2}$ where τ_Q is the timescale of the flavor-changing non-leptonic interactions and D_Q is the diffusion constant for flavor. The diffusion of strangeness towards the boundary and downness away from the boundary allows the strange matter at the boundary to have a strangeness fraction different from that of the nuclear matter which is undergoing deconfinement as the front moves.

In general, strangeness gradients could also exist in front of the boundary, as strangeness could diffuse through the boundary, creating (or adding to) hyperons

on the nuclear matter side. However, following Ref. [33], we will assume that the front moves fast enough for this effect to be negligible, so $\mu_K = 0$ everywhere ahead of the moving front, i.e. at $x < 0$. The conversion region is then limited to $x > 0$, and can be characterized by $\mu_K(x)$, or equivalently by the K-fraction parameter $a(x)$ which decreases with increasing strangeness fraction

$$a(x) \equiv \frac{n_K(x) - n_K^Q}{n_Q}, \quad (26)$$

where n_Q is the baryon number density in equilibrated strange quark matter, and the K density is $n_K^{Q^*}$ at $x = 0$ and as $x \rightarrow \infty$ it grows asymptotically to the constant value n_K^Q for equilibrated strange quark matter. From now on for simplicity we always assume that there are equal numbers of up, down and strange quarks in equilibrated quark matter ($n_K^Q = 0$). In equilibrated nuclear matter there are only up and down quarks (we assumed no hyperons in front of the boundary), so $n_K = n_d/2 = n_N$ for $x < 0$.

The spatial variation of a (Fig. 4, right panel) is determined by the steady-state transport equation, written in the rest frame of the boundary,

$$\begin{aligned} D_Q a'' - v_{\text{N} \rightarrow \text{Q}} a' - \mathcal{R}_Q(a) &= 0, \\ \mathcal{R}_Q(a) &= (\Gamma_{d \rightarrow s} - \Gamma_{s \rightarrow d})/n_Q, \end{aligned} \quad (27)$$

where D_Q is the flavor diffusion coefficient, $v_{\text{N} \rightarrow \text{Q}}$ the front speed and $\mathcal{R}_Q(a)$ is the net rate of flavor-changing weak interactions. The boundary conditions are

$$\begin{aligned} a(0^-) &= \frac{n_N}{n_Q} \equiv a_N, & a(x \rightarrow \infty) &\rightarrow 0, \\ a(0^+) &= \frac{n_K^{Q^*}}{n_Q} \equiv a_{Q^*}, & a'(0^+) &= -v_{\text{N} \rightarrow \text{Q}} \left(\frac{a_N - a_{Q^*}}{D_Q} \right). \end{aligned} \quad (28)$$

To understand the discontinuity in $a(x)$ across the boundary, let us consider how the chemical potentials vary in the conversion region. The left panel of Fig. 4 shows a schematic plot in the (μ_B, μ_K) plane. The parabolic-looking curve is the quark matter isobar for pressure $p_b > p_{\text{crit}}$. The square marked "N" is beta-equilibrated ($\mu_K = 0$) nuclear matter at the same pressure. The spatial variation in the conversion region, shown in the right panel of Fig. 4, can then be mapped on the chemical potential space as follows. At $x < 0$ we have beta-equilibrated nuclear matter (N). At $x = 0$, where $a(x)$ drops from a_N to a_{Q^*} , μ_K jumps to Q^* , which is out-of-equilibrium quark matter with non-zero μ_K , but at the same pressure as the nuclear matter. Then as we traverse the conversion region (increasing x), μ_K decays to zero, finally arriving at equilibrated quark matter (Q). All of these configurations are at the same pressure, based on the assumption that the thickness of the conversion region is negligible when compared to the radius of the star. The arrows along the $\mu_K = 0$ axis show how

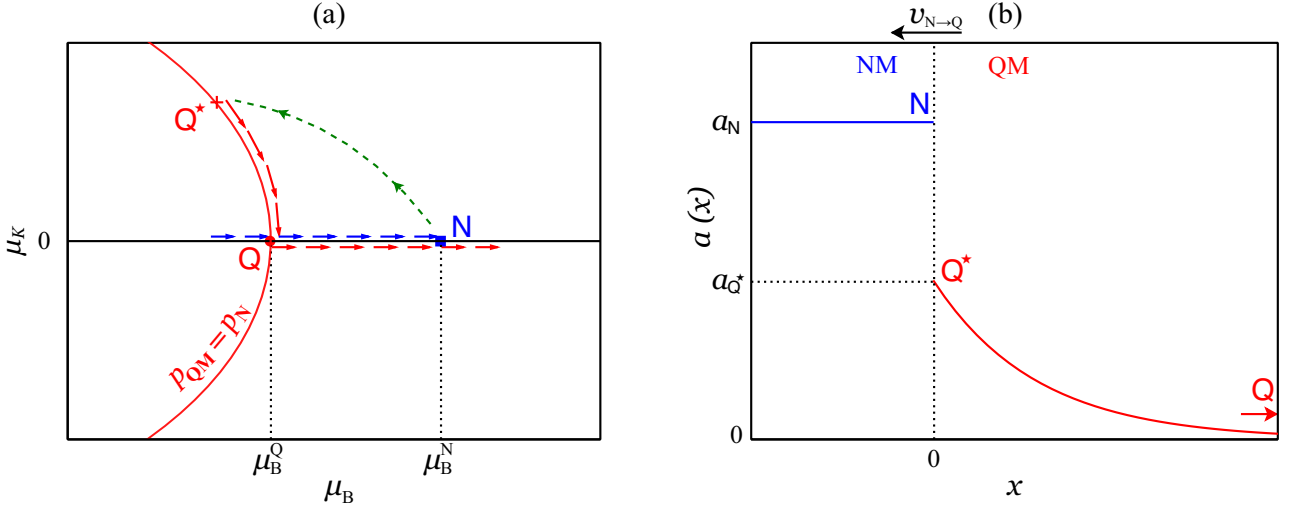


FIG. 4: (Color online) Conversion of nuclear matter into quark matter. Panel (b): spatial variation of the K-fraction parameter a (Eq. (26)) in the conversion region where the pressure is above p_{crit} (see Fig. 3). Panel (a): corresponding path in the (μ_B, μ_K) plane of chemical potentials. The quark matter isobar (red curve) is at the same pressure as the equilibrated nuclear matter (point N), and the arrows follow increasing pressure except from N to Q^* to Q where pressure is constant (traversing increasing x in the right panel).

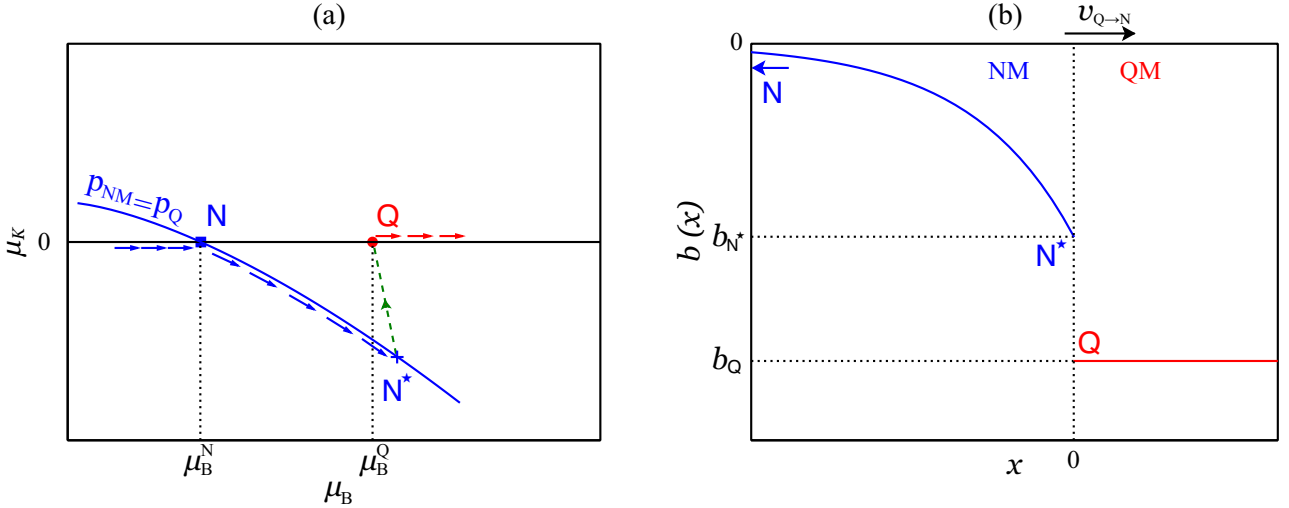


FIG. 5: (Color online) Conversion of quark matter into nuclear matter. Panel (b): spatial variation of the K-fraction parameter b (Eq. (46)) in the conversion region where the pressure is below p_{crit} (see Fig. 3). Panel (a): corresponding path in the (μ_B, μ_K) plane of chemical potentials. The nuclear matter isobar (blue curve) is at the same pressure as the equilibrated quark matter (point Q), and the arrows and the arrows follow increasing pressure except from N to N^* to Q where pressure is constant (traversing increasing x in the right panel).

μ_B varies as one moves larger distances through beta-equilibrated matter on either side of the conversion region, with the pressure rising monotonically. The arrows above the $\mu_K = 0$ axis (blue online) show μ_B increasing as we move inwards through nuclear matter until at N ($\mu_B = \mu_B^N$) we reach the phase boundary. After traversing the phase boundary and conversion region as described above, we are at Q, in beta-equilibrated quark matter at lower μ_B , and as we move into the quark core, μ_B rises

again (arrows below $\mu_K = 0$ axis, red online).

Olinto [33] argued that when the phase boundary is in a steady state of motion there is a “pileup” of nuclear matter in front so that nuclear and quark matter have the same density there, and the boundary has the same velocity relative to nuclear matter and quark matter, i.e. the nuclear matter near the boundary is stationary relative to the quark matter. However, we argue that this is not possible in steady state. When the phase boundary

moves, part of the star is transformed from lower density nuclear matter to denser quark matter, and hydrostatic equilibrium requires the star to shrink. This means that in the outer parts of the star the nuclear matter must fall inwards under gravity, so it is moving towards the quark matter. If the inward velocity of the nuclear matter went to zero near the phase boundary, this would require that the “pileup” grows with time, which is not a steady state situation. Instead, we argue that the baryon number conservation condition is automatically fulfilled because the weight of the outer region of the star pushes nuclear matter in to the front as fast as the front can “consume” it. The density of nuclear matter at the boundary is therefore unchanged by the movement of the boundary, and the nuclear matter velocity takes the value that is determined by baryon number conservation. As we saw in Eq. (12) this density step at the phase boundary is crucial for phase-conversion dissipation to occur ($a_N < 1$).

For a fixed value of a_{Q^*} , there is only one $v_{N \rightarrow Q}$ which guarantees a solution to Eq. (27) that satisfies the boundary conditions. To find the proper $v_{N \rightarrow Q}$, we apply the method in [33], which analogizes Eq. (27) to a classical mechanical problem and solves for the correct potential term, transforming the boundary value problem into an initial value problem. Taking into account both subthermal ($\mu_K \ll T$) and suprathreshold ($\mu_K \gg T$) regimes in the weak rate, the analytical approximation for the front speed in the NM \rightarrow QM half cycle is

$$v_{N \rightarrow Q} \simeq \sqrt{\frac{D_Q}{\tau_Q} \frac{a_{Q^*}^4 + 2\eta_Q a_{Q^*}^2}{2a_N(a_N - a_{Q^*})}} \quad (29)$$

where D_Q is the diffusion constant for flavor, τ_Q is the timescale of non-leptonic flavor-changing interactions, and η_Q gives the ratio of subthermal to suprathreshold rates. Eq. (29) is a generalization of Eq. (12) in Ref. [33], which is only valid in the suprathreshold regime. As we will see later on, a_{Q^*} is much less than a_N , therefore Eq. (29) becomes

$$v_{N \rightarrow Q} \simeq \frac{1}{a_N} \sqrt{\frac{D_Q}{2\tau_Q} \sqrt{a_{Q^*}^4 + 2\eta_Q a_{Q^*}^2}} \quad (30)$$

The full rate for the non-leptonic strangeness-changing process has been computed in [34], yielding

$$\mathcal{R}_Q(a) \simeq (a^3 + \eta_Q a)/\tau_Q, \quad (31)$$

$$\eta_Q = \frac{9\pi^2 T^2}{\mu_Q^2}, \quad (32)$$

$$\tau_Q = \left(\frac{128}{27 \cdot 5\pi^3} G_F^2 \cos^2 \theta_c \sin^2 \theta_c \mu_Q^5 \right)^{-1}, \quad (33)$$

where G_F is the Fermi constant, θ_c the Cabibbo angle, and therefore $\tau_Q \simeq 1.3 \times 10^{-9} \text{ s}$ ($300 \text{ MeV}/\mu_Q$)⁵; to leading order the diffusion coefficient (see Eqs. (28) and (36) in [35])

$$D_Q \simeq \frac{\pi q_D^{2/3}}{24 \alpha_s^2 h T^{5/3}} \quad (34)$$

where $h = \Gamma(\frac{8}{3})\zeta(\frac{5}{3})(2\pi)^{2/3} \simeq 1.81$, $\alpha_s = g^2/4\pi$ is the QCD coupling constant, and the Debye wave number for cold quark matter of three flavors is q_D where $q_D^2 = 3g^2\mu^2/(2\pi^2)$. The temperature dependence $T^{-5/3}$ comes from Landau damping that dominates for $T \ll \mu$ compared to the Debye screened case $D \propto T^{-2}$.

Different values of a_{Q^*} give different front profiles corresponding to different front velocities. There is an upper limit on a_{Q^*} which is constrained by the amplitude of external pressure oscillation, and the argument is as follows.

In order for the boundary to move, it must be favorable for neutrons to turn in to quarks at the boundary, so the total chemical potential per unit baryon number must be larger in beta-equilibrated nuclear matter (N in Fig. 4) than in out-of-equilibrium quark matter (Q^{*}) [50]

$$\mu_B^N > \mu_B^{Q^*} + \frac{n_K^{Q^*}}{n_{Q^*}} \cdot \mu_K^{Q^*} \quad (35)$$

On the isobar for quark matter, we parameterize the pressure at (μ_B, μ_K) as an expansion near equilibrium (Q)

$$p_{QM}(\mu_B, \mu_K) = p_Q + n_Q(\mu_B - \mu_B^Q) + n_K^Q(\mu_K - \mu_K^Q) + \frac{1}{2}\chi_K^Q(\mu_K - \mu_K^Q)^2 + \dots \quad (36)$$

where $\chi_K^Q \equiv \partial n_K / \partial \mu_K$ is the susceptibility with respect to K-ness evaluated at equilibrium (Q). In equilibrated quark matter, $\mu_K^Q = 0$. Since the whole conversion region is at the same pressure $p_{Q^*} = p_Q = p_b$, so solving for $\mu_B^{Q^*}$ we have

$$\mu_B^{Q^*} = \mu_B^Q - \left(\frac{n_K^Q}{n_Q} - \frac{\chi_K^Q \mu_K^{Q^*}}{2n_Q} \right) \cdot \mu_K^{Q^*}. \quad (37)$$

Assuming that Q^{*} is close to equilibrium, so that $n_K^{Q^*} \approx n_K^Q$, $n_{Q^*} \approx n_Q$, Eq. (35) becomes

$$\mu_B^N - \mu_B^Q > \frac{\chi_K^Q (\mu_K^{Q^*})^2}{2n_Q}. \quad (38)$$

From Eq. (28), $a_{Q^*} = n_K^{Q^*}/n_{Q^*} \approx \mu_K^{Q^*} \chi_K^Q/n_Q$, then Eq. (38) leads to an upper bound on a_{Q^*}

$$a_{Q^*}^{\max} = \sqrt{\frac{2\Delta\mu_B \chi_K^Q}{n_Q}}, \quad (39)$$

with

$$\Delta\mu_B \equiv \mu_B^N - \mu_B^Q \simeq (\gamma - 1)\delta p/n_Q, \quad (40)$$

where $\delta p = |p_b - p_{\text{crit}}| \geq 0$ (Fig. 3) and $\gamma \equiv n_Q/n_N = 1/a_N$. Notice that the derivation of Eq. (39) is totally general and can also be applied to matter with nonzero n_K at equilibrium (see Sec. IV C).

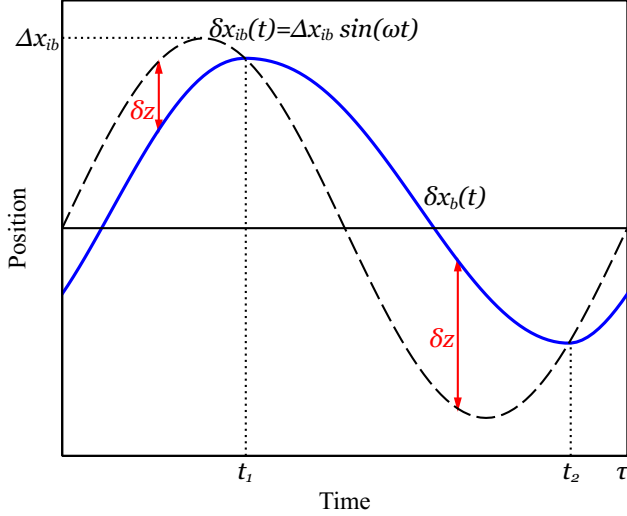


FIG. 6: (Color online) Diagram showing how the ideal boundary position (dashed line) and the real boundary position (solid (blue) line) vary in time. The ideal boundary is where the phase boundary would be if the phase conversion process equilibrated instantaneously, and it is determined by the instantaneous external pressure (Eq. (9)). The real boundary is always “chasing” the ideal boundary, with velocity given by Eq. (42) and (59) where $\delta z(t)$ is its distance from the ideal boundary. The real boundary coincides with the ideal boundary twice per cycle, at $t = t_1$ and $t = t_2$.

The pressure oscillation is related to how far the real boundary is away from its ideal position via

$$\delta p = g_b \varepsilon_{\text{crit}}^N (\delta x_{ib}(t) - \delta x_b(t)), \quad (41)$$

where the ideal position $\delta x_{ib}(t) = \Delta x_{ib} \sin(\omega t)$, and the amplitude $\Delta x_{ib} = \Delta p_N / g_b \varepsilon_{\text{crit}}^N$ (see Eq. (9)). If we assume that the boundary is always moving at its maximum speed ($a_{Q^*} \approx a_{Q^*}^{\text{max}}$), then according to Eq. (30) and Eq. (39)–(41) the velocity of the boundary in the $\text{NM} \rightarrow \text{QM}$ half cycle ($t < t_1$ and $t > t_2$ in Fig. 6) is determined by

$$\frac{d\delta x_b}{dt} \simeq \frac{1}{a_N} \sqrt{\frac{D_Q}{2\tau_Q}} \sqrt{[\delta z / \ell_Q]^2 + 2\eta_Q \delta z / \ell_Q} \quad (42)$$

where $\delta z \equiv |\delta x_{ib} - \delta x_b|$ is how far the boundary is from its equilibrium position at the current pressure (see Fig. 6), and ℓ_Q characterizes its typical length

$$\ell_Q = \frac{(n_Q / \chi_K^Q) n_Q}{2(\gamma - 1) g_b \varepsilon_{\text{crit}}^N}. \quad (43)$$

C. Conversion of quark matter into nuclear matter

The conversion from quark matter to nuclear matter has not been analyzed previously because it does not

arise if strange matter is stable at zero pressure, which is the context in which previous analyses were performed. However, it can analogously be described in terms of conversion and diffusion behind the boundary, now on the hadronic side where strangeness is carried by hyperons. There are various hyperons that could be present in dense hadronic matter and correspondingly multiple weak reactions involving these hyperons. For an illustrative calculation we only consider one such process, $n + n \rightarrow p + \Sigma^-$, which is a reasonable choice because Σ^- hyperons are expected to be among the first to appear when nuclear matter is compressed, see e.g. [36]. For simplicity, we also neglect electrons in the system, which is admittedly not a good approximation, but we are only aiming to provide an illustrative example. In this case

$$\mu_K = 2\mu_n - \mu_p - \mu_\Sigma \quad (44)$$

$$n_K = \frac{1}{6}(2n_n - n_p - n_\Sigma). \quad (45)$$

Moving away from the boundary on the hadronic side, into the conversion region, the K density is $n_K^{N^*}$ at $x = 0$ and as $x \rightarrow -\infty$ it grows asymptotically to the nonzero constant value $n_K^N \simeq n_n/3 \approx n_N/3$ for equilibrated nuclear matter with Σ^- hyperons, where n_N is the baryon number density in equilibrated nuclear matter. As before we neglect strangeness conversion ahead of the boundary, which is the quark matter region in this case. In equilibrated quark matter we assume there are equal numbers of up, down and strange quarks, so $n_K = 0$ for $x > 0$.

As in Sec. IV B we define a parameter to characterize the deviation of the K fraction from its equilibrium value,

$$b(x) \equiv \frac{n_K(x) - n_K^N}{n_N} \quad (46)$$

and the steady-state transport equation for $b(x)$ in the rest frame of the boundary is

$$D_N b'' - v_{Q \rightarrow N} b' - \mathcal{R}_N(b) = 0, \quad (47)$$

$$\mathcal{R}_N(b) = (\Gamma_{n+n \rightarrow p+\Sigma^-} - \Gamma_{p+\Sigma^- \rightarrow n+n}) / n_N, \quad (48)$$

where D_N is the flavor diffusion coefficient, $v_{Q \rightarrow N}$ is the front speed for the $\text{QM} \rightarrow \text{NM}$ transition and $\mathcal{R}_N(b)$ the strangeness-changing reaction rate divided by the baryon number density in nuclear matter. The boundary conditions are

$$\begin{aligned} b(0^-) &= \frac{n_K^{N^*} - n_K^N}{n_N} \equiv b_{N^*}, & b(x \rightarrow -\infty) &\rightarrow 0, \\ b(0^+) &= \frac{-n_K^N}{n_N} \equiv b_Q, & b'(0^-) &= v_{Q \rightarrow N} \left(\frac{b_Q - b_{N^*}}{D_N} \right). \end{aligned} \quad (49)$$

The right panel of Fig. 5 shows how $b(x)$ varies through the phase boundary and transition region. The left panel of Fig. 5 shows schematically the behavior in the (μ_B, μ_K) plane. The short curve through N and N^* is the nuclear matter isobar for pressure $p_b < p_{\text{crit}}$. The dot marked

“Q” is beta-equilibrated quark matter at the same pressure, which exists (see right panel) at $x = 0^+$. The point N^* is out-of-equilibrium nuclear matter which is found just behind the boundary at $x = 0^-$. The point N is beta-equilibrated nuclear matter, which is found at the tailing end of the conversion region. All these forms of matter are at the same pressure as long as thickness of the conversion region is much smaller than the radius of the star. The arrows represent how the chemical composition changes as one moves from the hadronic outer part of the star through the conversion region to the quark core. At the boundary $\mu_B^N < \mu_B^Q$ and μ_K in out-of-equilibrium nuclear matter is negative because of the presence of massive hyperons.

Following the same logic as in the previous section, we find the analytic approximation for the velocity of the boundary

$$v_{Q \rightarrow N} \simeq -\sqrt{\frac{D_N}{\tau_N} \frac{b_{N^*}^4 + 2\eta_N b_{N^*}^2}{2b_Q(b_Q - b_{N^*})}} \xrightarrow{|b_{N^*}| \ll |b_Q|} \frac{1}{b_Q} \sqrt{\frac{D_N}{2\tau_N}} \sqrt{b_{N^*}^4 + 2\eta_N b_{N^*}^2}, \quad (50)$$

where $-b_Q \lesssim 1/3$. The full rate for the weak interaction has been computed in [6]

$$\mathcal{R}_N(b) \simeq (b^3 + \eta_N b)/\tau_N, \quad (51)$$

$$\eta_N = \frac{4\pi^2 T^2 (\chi_K^N)^2}{n_N^2} \quad (52)$$

and the time scale

$$\tau_N = \left[\frac{-2\chi G_F^2}{3 \cdot (2\pi)^5} \cos^2 \theta_c \sin^2 \theta_c m_n^{*2} m_p^* m_\Sigma^* k_F^\Sigma n_N^2 (\chi_K^N)^{-3} \right]^{-1}, \quad (53)$$

where χ is determined by the reduced symmetric and antisymmetric coupling constants with typical value ~ 0.1 and $\chi_K^N \equiv \partial n_K / \partial \mu_K$ is evaluated at nuclear matter in equilibrium (N). Both k_F^Σ and χ_K^N are functions of n_N , depending on the nuclear matter EoS. The timescale for relevant weak interactions to happen in nuclear matter is much longer than that in quark matter (Eq. (33)), because the baryons are non-relativistic and their densities are lower. For typical transition densities in hybrid stars we studied, the ratio τ_N/τ_Q is of order 10^2 .

To estimate the diffusion coefficient $D_N \simeq \frac{1}{3} v_N \lambda_N$ we estimate v_N by the Fermi velocity of hyperons ($v_N \simeq v_F^\Sigma = k_F^\Sigma/m_\Sigma^*$), and the mean free path by $\lambda_N \simeq v_F^\Sigma/\nu_{n\Sigma}$, where $\nu_{n\Sigma}$ is the hadron/hyperon collision frequency similar to the hadron/hadron collision frequency ν_{np} (see Eq. (55) of [37]). As a result,

$$D_N \simeq \frac{m_n^2 k_F^{\Sigma 2}}{32 m_n^* m_\Sigma^{*4} T^2 S_{n\Sigma}(k_F^n, k_F^\Sigma)}, \quad (54)$$

where $S_{n\Sigma}$ is the effective hadron/hyperon scattering cross section which we for simplicity approximate by

the proton/neutron cross section given in Eq. (58) of [37]. Given the nuclear matter EoS, k_F^Σ and $S_{n\Sigma}$ can be expressed in terms of the baryon density n_N . The strangeness diffusion coefficient in nuclear matter is typically much smaller than in quark matter (Eq. (34)), because hadrons and hyperons are non-relativistic while quarks are moving nearly at the speed of light, and also because the long-range interactions between the quark interactions give the different temperature dependence $D_N/D_Q \propto (T/\mu)^{1/3}$. At temperatures relevant to neutron stars, this ratio is of order 10^{-2} .

The K-fraction in nuclear matter at the boundary with quark matter, b_{N^*} , is constrained by how far out of equilibrium the boundary is. For the boundary to move towards its “ideal” position the total chemical potential per baryon number in beta-equilibrated quark matter (Q in Fig. 4) must be larger than that in the non-beta-equilibrated nuclear matter on the other side of the boundary (N^*). Following the same logic as in Sec. IV B we obtain a condition similar to Eq.(38)

$$\mu_B^Q - \mu_B^N > \frac{(-\mu_K^{N^*})^2 \chi_K^N}{2n_N}. \quad (55)$$

From Eq. (49), $b_{N^*} = -n_K^{N^*}/n_N \approx -\mu_K^{N^*} \chi_K^N/n_N$, so Eq. (55) gives an upper bound on $-b_{N^*}$ and hence on the front speed $v_{Q \rightarrow N}$

$$(-b_{N^*})^{\max} = \sqrt{\frac{2\Delta\mu_B \chi_K^N}{n_N}}, \quad (56)$$

$$\Delta\mu_B = \mu_B^Q - \mu_B^N \simeq (\gamma - 1)\delta p/n_Q, \quad (57)$$

where

$$\delta p = g_b \varepsilon_{\text{crit}}^N (\delta x_b(t) - \Delta x_{ib} \sin(\omega t)). \quad (58)$$

Assuming that the boundary moves at its maximum speed, $(-b_{N^*}) \approx (-b_{N^*})^{\max}$, the boundary velocity in the QM \rightarrow NM half cycle ($t_1 < t < t_2$ in Fig. 6) is

$$\frac{d\delta x_b}{dt} \simeq \frac{1}{b_Q} \sqrt{\frac{D_N}{2\tau_N}} \sqrt{[\delta z/\ell_N]^2 + 2\eta_N \delta z/\ell_N} \quad (59)$$

where $\delta z \equiv |\delta x_b - \delta x_{ib}|$ is how far the boundary is from its equilibrium position at the current pressure, with the typical length

$$\ell_N = \frac{(n_N/\chi_K^N)n_Q}{2(\gamma - 1)g_b \varepsilon_{\text{crit}}^N}. \quad (60)$$

Therefore with the periodic condition $\delta x_b(t) = \delta x_b(2\pi/\omega + t)$, Eq. (42) and Eq. (59) fully specify the movement of the phase boundary in response to the external pressure oscillation. Next we compute the energy dissipation in this process and see whether it is capable of saturating the r-mode.

D. Dissipated power and saturation amplitude

From Sec. III B we know that during one cycle of an r-mode of amplitude α the energy dissipated in a radially oriented cylinder with an infinitesimal base area dS straddling the phase boundary at (θ, ϕ) is

$$dW(\alpha, \theta, \phi) = dS (\gamma - 1) \Delta p_N \int_0^\tau \cos(2\phi + \omega t) \frac{d\delta R_b}{dt} dt \quad (61)$$

where the position of the phase boundary $\delta R_b(t)$ is the same as $\delta x_b(t)$ in Sec. IV B and Sec. IV C, which we assume to move at its maximal speed (see Eqs. (42) and (59)), and $dS = \bar{R}_b^2 \sin\theta d\theta d\phi$. From Eq. (24)

$$\Delta p_N = g_b \varepsilon_{\text{crit}}^N |\delta R_{ib}| = \varepsilon_{\text{crit}}^N C_b \alpha |\sin^2\theta \cos\theta| \quad (62)$$

Integrating Eq. (61) over solid angle gives the total dissipation of the r-mode in one cycle of oscillation and hence the total power dissipated P_{dis} . The r-mode amplitude stops growing (saturates) when this equals the power injected via back-reaction from gravitational radiation P_{gr} .

As an illustrative example, Fig. 7 shows the dissipated power as a function of r-mode amplitude for a hybrid star rotating with frequency $f = 600$ Hz, with quark core size $\bar{R}_b/R = 0.56$ and temperature $T = 10^8$ K. For the quark matter EoS we use the CSS parameterization [38] with $n_{\text{trans}} = 4n_0$, $\Delta\varepsilon/\varepsilon_{\text{trans}} = 0.2$, and $c_{\text{QM}}^2 = 1$. The hadronic matter EoS is taken from Ref. [39].

In the subthermal regime, the dissipated power first rises with the r-mode amplitude α as α^3 at very low amplitude, before entering a resonant region with a maximum in P_{dis}/α^2 . At high amplitude in the suprathreshold regime, the dissipated power is proportional to α^2 . The power in gravitational radiation from the r-mode P_{gr} (Eq. (A17)) rises as α^2 , and is also shown in Fig. 7 for this particular hybrid star. At low amplitude, the phase conversion dissipation is suppressed relative to the gravitational radiation, and therefore plays no role in damping the r-mode. If other damping mechanisms are too weak to suppress the r-mode, its amplitude will grow. However, as the amplitude grows the phase conversion dissipation becomes stronger, and in this example there is a saturation amplitude α_{sat} at which it equals the gravitational radiation, and the mode stops growing.

Varying parameters such as the size of the quark matter core, rotation frequency or temperature of the star, etc, will shift the curves in Fig. 7, and if the phase conversion dissipation is too weak then there will be no intersection point (P_{gr} will be greater than P_{dis} at all α) and phase conversion dissipation will not stop the growth of the mode. However, we can see from Fig. 7 that if saturation occurs, the resultant α_{sat} is in the low-amplitude regime, where an analytical approach is available, and the saturation amplitude is extraordinarily low, of order 10^{-12} . This is typical of all model hybrid stars that we investigated. In Appendix A we derive the analytical expression for the dissipated power in the low-amplitude

regime (dashed (black) line in Fig. 7), obtaining

$$P_{\text{dis}}^{\text{sub}}(\alpha) \approx \frac{\alpha^3}{15} \left(\frac{105}{756\pi} \right)^{3/2} \frac{\gamma - 1}{\Delta \tilde{p}_N} \frac{(\varepsilon_{\text{crit}}^N)^2 \Omega^7 \bar{R}_b^{11}}{g_b R^3}. \quad (63)$$

This expression allows us to assess how the strength of phase conversion dissipation depends on the various parameters involved. It is particularly sensitive to the size of the quark core, and this will be important when considering a whole family of hybrid stars with different central pressures and hence different core sizes.

The results of such an investigation are shown in Fig. 8, where the solid (red) curve gives the numerically calculated saturation amplitude (α_{sat} in Fig. 7) as a function of the size of the quark matter core in units of the star radius, \bar{R}_b/R . To construct this curve we used the hadronic and quark matter EoS of Fig. 7 and varied the central pressure, yielding a family of different star configurations. As \bar{R}_b/R decreases, the dissipation power P_{dis} decreases rapidly relative to the gravitational radiation P_{gr} . The relative shift in the two corresponding curves in Fig. 7 leads to an upper limit on α_{sat} when P_{gr} is tangent to P_{dis} . This corresponds to the end of the solid curve in Fig. 8 at $\alpha_{\text{sat}}^{\text{max}}$ at the critical value of the quark core size, $(\bar{R}_b/R)_{\text{crit}}$, below which the phase-conversion mechanism cannot saturate the r-mode any more.

The black dashed curve in Fig. 8 is the low-amplitude analytical approximation to α_{sat} (see also Appendix A, Eq. (A20)),

$$\begin{aligned} \alpha_{\text{sat}}^{\text{approx}} &= \left(\frac{2^{22} \pi^{9/2}}{3^3 \cdot 5^{5/2}} \right) G \frac{\tilde{D}_N}{\tau_N} \frac{(\chi_K^N)^3}{n_Q n_N^3 b_Q^2} \frac{g_b^3 M^2 \tilde{J}^2}{\Omega} \frac{R^9}{\bar{R}_b^{11}} \\ &\approx 4.2 \times 10^{-11} \gamma \left(\frac{\tilde{D}_N}{1.5 \text{ MeV}^3} \right) \left(\frac{\tau_N}{2 \times 10^{-8} \text{ s}} \right)^{-1} \\ &\times \left(\frac{b_Q}{1/3} \right)^{-2} \left(\frac{n_N}{2n_0} \right)^{-4} \left(\frac{\chi_K^N}{(100 \text{ MeV})^2} \right)^3 \left(\frac{g_b}{g_u} \right)^3 \\ &\times \left(\frac{\varepsilon_{\text{crit}}^Q}{2 \varepsilon_{\text{crit}}^N} \right)^3 \left(\frac{\varepsilon_{\text{crit}}^N}{600 \text{ MeV fm}^{-3}} \right)^3 \left(\frac{M}{1.4 M_\odot} \right)^2 \\ &\times \left(\frac{\tilde{J}}{0.02} \right)^2 \left(\frac{f}{1 \text{ kHz}} \right)^{-1} \left(\frac{R}{10 \text{ km}} \right) \left(\frac{\bar{R}_b/R}{0.4} \right)^{-8} \quad (64) \end{aligned}$$

where $D_N \equiv \tilde{D}_N \cdot T^{-2}$ (see Eq. (54)), and g_u is the Newtonian gravitational acceleration at the phase boundary when the quark core has uniform density $\varepsilon = \varepsilon_{\text{crit}}^Q$ ($g_u \equiv \frac{4}{3} \pi G \varepsilon_{\text{crit}}^Q \bar{R}_b$). This approximation is very accurate when the phase conversion damping is strong, but it does not capture the sudden weakening of that dissipation when, for example, the core radius becomes small. It is therefore useful to have some idea of its range of validity.

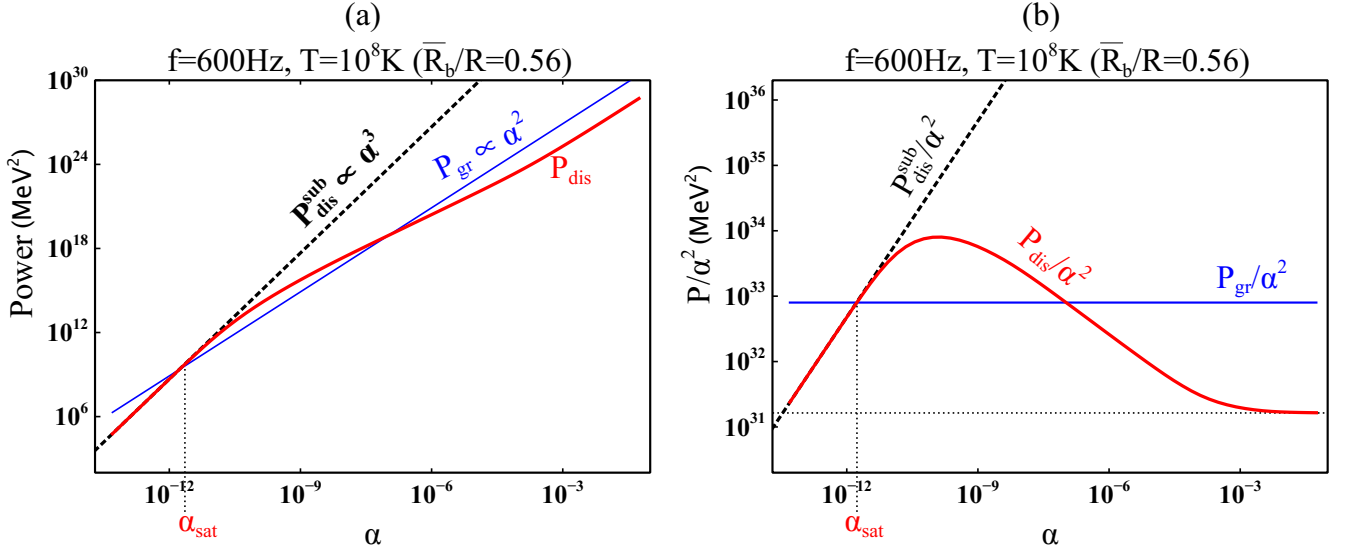


FIG. 7: (Color online) Panel (a) shows dissipated power due to phase conversion P_{dis} (thick solid red curve) as a function of r-mode amplitude α for a specific example hybrid star (see text). Panel (b) shows the same quantity where the vertical axis now shows the ratio P_{dis}/α^2 . At first P_{dis} is proportional to α^3 at very low amplitude (dashed line), then at some intermediate amplitude varies less quickly, with a maximum in P_{dis}/α^2 , and finally changes to α^2 at higher amplitude. Also shown is gravitational radiation power P_{gr} (thin solid blue straight line) which is proportional to α^2 at all amplitudes. The r-mode amplitude will stop growing when dissipation balances radiation, at the first point of intersection between the two curves. This defines the saturation amplitude α_{sat} .

E. Range of validity of low-amplitude approximation

The range of validity of Eqs. (63) and (64) is found by calculating the next-to-leading (NLO) contribution, and requiring that it be less than a fraction ϵ of the total dissipated power. We find (see Appendix B) that the approximation is valid when

$$\begin{aligned} \epsilon &\geq \frac{2^{39}\pi^5}{3^{12}5^4} \frac{G^2}{(\gamma-1)^2} \frac{g_b M^4 \tilde{J}^4 \Omega^6}{(\varepsilon_{\text{crit}}^{\text{N}})^2} \left(\frac{R}{\bar{R}_b}\right)^{16} \\ &\simeq 2.96 \left(\frac{\gamma-1}{0.5}\right)^{-2} \left(\frac{\varepsilon_{\text{crit}}^{\text{Q}}}{2\varepsilon_{\text{crit}}^{\text{N}}}\right)^2 \left(\frac{g_b}{g_u}\right)^2 \left(\frac{M}{1.4M_\odot}\right)^4 \\ &\times \left(\frac{\tilde{J}}{0.02}\right)^4 \left(\frac{f}{1\text{ kHz}}\right)^6 \left(\frac{R}{10\text{ km}}\right)^2 \left(\frac{\bar{R}_b/R}{0.4}\right)^{-14}. \end{aligned} \quad (65)$$

We see that the validity of the low-amplitude approximation is mainly determined by the size of the quark matter core and the rotation frequency of the star.

V. CONCLUSION

We have described how phase conversion in a multi-component compact star provides a mechanism for damping density oscillations, via the phase lag in the response of the interface between components of different baryon densities to the applied pressure oscillation. The phase lag arises from the finite rate of interconversion between

the phases, which limits the speed with which the interface can move. We studied the case where the two phases are separated by a sharp boundary (first order phase transition) and analyzed the movement of the interface in the approximation of a steady state, neglecting additional acceleration effects and complicated hydrodynamic effects like turbulence. In particular, we studied the astrophysically interesting case of the damping of r-mode oscillations [17, 18] in a two-component star. We found that phase conversion dissipation does not affect the r-mode instability region, because it vanishes as α^3 at low r-mode amplitude α . However, depending on the values of relevant parameters, phase conversion dissipation can either saturate the r-mode at extremely low amplitudes, $\alpha_{\text{sat}} \lesssim 10^{-10}$ in the explicit example of hadron-quark transformation at the sharp quark-hadron interface in a hybrid star, or be insufficient to saturate the r-mode at all. The reason for this behavior stems, analogously to the bulk viscosity [25], from the resonant character of the dissipation, which is relatively strong when the time scale of the dissipation matches the time scale of the external oscillation (see Fig. 7). Whether saturation is possible depends therefore on the microscopic and astrophysical parameters, like in particular on the mass of the quark core which should not be too small.

Our main result is (61), which must be evaluated using numerical solutions of (42) and (59). We also give the low-amplitude analytic expressions for the power dissipated (63) and the saturation amplitude (64) which are valid when the dissipation is sufficiently strong, obeying

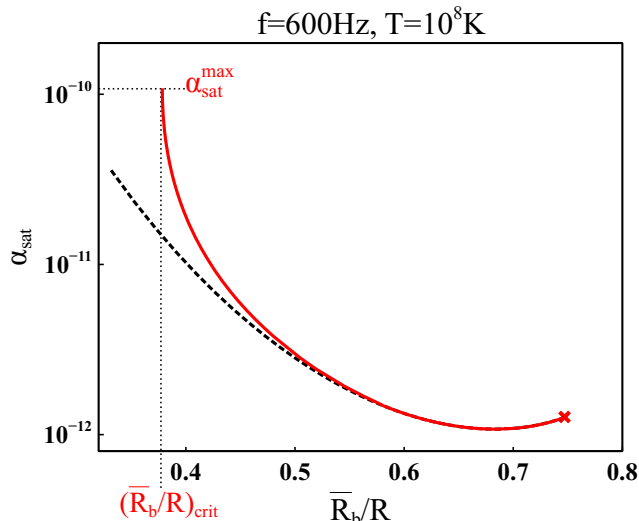


FIG. 8: (Color online) R-mode saturation amplitude (red solid curve) and its low-amplitude analytical approximation (black dashed curve) as a function of the radius of the quark matter core \bar{R}_b divided by the star radius R in a family of hybrid stars. For $\bar{R}_b/R < (\bar{R}_b/R)_{\text{crit}} \approx 0.38$, damping is too weak to saturate the r-mode. At $\bar{R}_b/R \gtrsim 0.75$ the hybrid star is unstable against gravitational collapse. The mass fraction of the core is in the range $0.12 \lesssim M_{\text{core}}/M_{\text{star}} \lesssim 0.68$ for all the configurations shown on the red solid curve.

(65) with $\epsilon \ll 1$.

Our results have significant implications for astrophysical signatures of exotic high-density phases of matter, such as quark matter. The observed data for millisecond pulsars is not consistent with the minimal model of pulsars as stars made of nuclear matter with damping of r-modes via bulk and shear viscosity [40]. Resolving this discrepancy requires either a new mechanism for stabilizing r-modes, or a new mechanism for saturating unstable r-modes at $\alpha_{\text{sat}} \lesssim 10^{-8} - 10^{-7}$ [40–42]. Previously proposed mechanisms have problems to achieve this. Suprathreshold bulk viscosity and hydrodynamic oscillations both give $\alpha_{\text{sat}} \sim 1$ [19, 22]. The non-linear coupling of the r-mode to viscously damped daughter modes could give $\alpha_{\text{sat}} \sim 10^{-6}$ to 10^{-3} [23, 43]. The recently proposed vortex/fluxtube cutting mechanism [24] might give sufficiently small saturation amplitudes but is present only at sufficiently low temperatures $T \ll T_c \lesssim 10^9$ K, which could be exceeded by the r-mode (and/or accretion) heating [40]. One of the main results of this paper is that phase conversion dissipation can provide saturation at the required amplitude to explain millisecond pulsar data.

Secondly, due to the extremely low r-mode saturation amplitude of our proposed mechanism hybrid stars would behave very differently from neutron or strange stars. As discussed in [40], if the known millisecond sources were hybrid stars then, for the low saturation amplitudes that we have found, they would have cooled out of the

r-mode instability region quickly (in millions of years) so that they would have very low temperatures by now. In contrast, in neutron stars r-modes would be present and would provide such strong heating that the temperature of observed millisecond pulsars would be $T_\infty \sim O(10^5 - 10^6)$ K [40]. This prediction assumes a (so far unknown) saturation mechanism that would saturate the mode at a value $\alpha_{\text{sat}} \lesssim 10^{-8}$ required by the pulsar data. This temperature is significantly higher than what standard cooling estimates suggest for such old sources. The same holds for strange quark stars where the enhanced viscous damping can explain the pulsar data, but even in this case the star would spin down along the boundary of the corresponding stability window which would keep it at similarly high temperatures. Measurements of or bounds on temperatures of isolated millisecond pulsars provide therefore a promising way to discriminate hybrid stars.

Our analysis considered only strangeness-changing non-leptonic processes when we discussed the hadron-quark transformation as an example of phase conversion dissipation. However, there are also leptonic processes that equilibrate the non-strange neutron-proton or up-down ratio. For ordinary bulk viscosity in hadronic or quark matter these processes are only relevant at temperatures far above the temperature of a neutron star because their rate is parametrically smaller than the strangeness changing rate discussed here by a factor of $(T/\mu)^2$ [2]. However, leptonic processes might play an important role in phase conversion dissipation because hadronic matter has more electrons and up quarks than quark matter, so, just as for strangeness, there will be a conversion region behind the moving boundary where conversion and diffusion of up-ness is occurring. Taking this into account could change the estimates given here and should be studied in more detail in the future.

As well as the quark-hadron interface in a hybrid star, any first-order phase transition that leads to a sharp interface between two phases with different baryon densities could, via the mechanism discussed here, cause dissipation of global pressure oscillation modes. One possibility would be different phases of quark matter, perhaps with different Cooper pairing patterns, such as the color-flavor locked (CFL) phase, the 2-flavor color superconductor (2SC) or various forms of inhomogeneous and asymmetric pairing [44], which are all generally connected by first order phase transitions. Because cross-flavor pairing induces shifts in the Fermi surfaces of the participating species, different color superconducting phases will often have different flavor fractions, so movement of the interface between them requires weak interactions, as in the case of the quark-hadron interface. The dissipation mechanism discussed here may therefore be expected to operate, albeit mildly suppressed by the smallness of the baryon number density differences between these phases.

Our discussion was limited to the case of a sharp interface, which is the expected configuration if the surface tension is large enough. If the surface tension is

small there will instead be a mixed phase region where domains of charged hadronic and quark matter coexist [45, 46]. We expect that the phase conversion dissipation mechanism will operate in this case too, as the domains expand and shrink in response to pressure oscillations. However, to estimate this contribution is far more complicated since it requires us to consider the dynamic formation, growth, and merging of these structures, taking into account the costs and gains due to surface tension and electric field energy. Such an analysis is far beyond the scope of this work, but we expect that the dissipation due to such transformations will be roughly comparable to the estimates given here. A similar mechanism should also be relevant for the “nuclear pasta” mixed phases in the inner crust of an ordinary neutron star. In this case in addition to the slow beta equilibration processes there may also be slow strong interaction equilibration processes, whose rate is suppressed by tunneling factors for the transition between geometric domains of different size. This could further enhance the dissipation.

The phase conversion mechanism for damping relies on the transition between two phases being first order. If there is a crossover then dissipation due to particle conversion is described by the standard bulk viscosity. Examples are the appearance of hyperons in the dense interior or the crossover from npe to $npe\mu$ hadronic matter, where the conserved particle density is lepton number instead of baryon number [47]. The conversion is then not restricted to a thin transition region and partial conversion giving rise to bulk viscosity dissipation takes place all over the relevant part of the star. The additional effect, that the size of the region where muons are present changes as well, is negligible, since the muon fraction continuously goes to zero. This is also reflected by the vanishing of the prefactor in the parenthesis of our general expressions Eq. (12).

In this work, we obtained a reasonable first estimate of the size of the damping by treating the movement of the phase boundary in the steady-state approximation [33], assuming that it can accelerate arbitrarily fast and that it can move as fast as allowed by general thermodynamic constraints. In reality the acceleration of the phase boundary near the turning points of its motion might be further slowed down by the fact that the steady-state conversion region has to form, and if it therefore cannot accelerate fast enough there will be additional dissipation during this part of the cycle, even if the phase boundary is eventually fast enough to stay in chemical equilibrium near the equilibrium position. Our analysis showed that even being out of chemical equilibrium for only a small fraction of a cycle causes the system to dissipate a huge amount of energy, so it is possible that including these additional acceleration effects may yield an even lower r-mode saturation amplitude and saturate r-modes even in stars with small quark cores. Including the realistic acceleration of the phase boundary will require solving the full time dependent evolution of the phase conversion front. Similarly, it is likely that turbulence plays a major

role in the phase conversion, as found in several analyses [31, 32, 48] of the one-time burning of a (meta-stable) neutron star. The inclusion of these complications is an interesting future project.

Appendix A: Angular integral and saturation amplitude in the subthermal regime

To determine the velocity of the boundary in the NM \rightarrow QM half cycle, we define a dimensionless parameter $y(\varphi) \equiv \delta x_b / \Delta x_{ib}$ with $\varphi = \omega t$, then Eq. (42) becomes

$$\left(\frac{dy}{d\varphi}\right)_{N \rightarrow Q} \simeq A_Q \sqrt{\rho_Q (\sin \varphi - y)^2 + (\sin \varphi - y)} \quad (\text{A1})$$

where A_Q represents an overall amplitude of the speed

$$A_Q = \frac{3}{a_N} \sqrt{\frac{D_Q}{2\tau_Q} \frac{(\gamma - 1)\eta_Q}{(n_Q/\chi_K^Q)n_Q} \frac{g_b \varepsilon_{\text{crit}}^N}{\Omega \sqrt{\Delta p_N}}}, \quad (\text{A2})$$

while ρ_Q is the ratio of suprathreshold to subthreshold contribution

$$\rho_Q = \frac{(\gamma - 1)\Delta p_N}{\eta_Q (n_Q/\chi_K^Q)n_Q}. \quad (\text{A3})$$

Similarly in the QM \rightarrow NM half cycle Eq. (59) becomes

$$\left(\frac{dy}{d\varphi}\right)_{Q \rightarrow N} \simeq A_N \sqrt{\rho_N (\sin \varphi - y)^2 + (\sin \varphi - y)} \quad (\text{A4})$$

and the two coefficients are

$$A_N = \frac{3}{b_Q} \sqrt{\frac{D_N}{2\tau_N} \frac{(\gamma - 1)\eta_N}{(n_N/\chi_K^N)n_Q} \frac{g_b \varepsilon_{\text{crit}}^N}{\Omega \sqrt{\Delta p_N}}}, \quad (\text{A5})$$

$$\rho_N = \frac{(\gamma - 1)\Delta p_N}{\eta_N (n_N/\chi_K^N)n_Q}. \quad (\text{A6})$$

Combining Eq. (A1) and Eq. (A4), and setting $s(\varphi) \equiv \sin \varphi - y(\varphi)$ we have

$$\cos \varphi - \frac{ds}{d\varphi} = \begin{cases} A_{N \rightarrow Q} \sqrt{\rho_Q s(\varphi)^2 + s(\varphi)}, & s(\varphi) \geq 0, \\ A_{Q \rightarrow N} \sqrt{\rho_N s(\varphi)^2 - s(\varphi)}, & \text{otherwise.} \end{cases} \quad (\text{A7})$$

With the periodic condition ($s(\varphi) = s(2\pi + \varphi)$), one can solve for the full profile of the interface position and continue to calculate the dissipated energy.

The total dissipation of the r-mode in one cycle of the oscillation is

$$W(\alpha) = \int_0^\pi \int_0^{2\pi} dS (\gamma - 1) \frac{(\Delta p_N)^2}{g_b \varepsilon_{\text{crit}}^N} V(\Delta p_N) \quad (\text{A8})$$

where the integral $V(\Delta p_N)$ depends on the velocity of the boundary in both directions

$$V(\Delta p_N) \equiv \int_0^{2\pi} \sin \varphi \frac{d(\sin \varphi - s)}{d\varphi} d\varphi \quad (\text{A9})$$

and $s(\varphi)$ is the solution to Eq. (A7). In general this integral can be computed numerically as long as coefficients A 's and ρ 's in the differential equation Eq. (A7) are known.

At small oscillation when Δp_N is tiny, however, the subthermal regime dominates ($\rho_Q, \rho_N \ll 1$) and Eq. (A7) can be simplified as

$$\cos \varphi - \left(\frac{ds}{d\varphi} \right)_{\text{sub}} = \begin{cases} A_Q \sqrt{s(\varphi)}, & s(\varphi) \geq 0, \\ A_N \sqrt{-s(\varphi)}, & \text{otherwise.} \end{cases} \quad (\text{A10})$$

Since both A_Q and A_N are much greater than 1, to leading order the analytical solution to Eq. (A10) is

$$s(\varphi) = \Theta(\cos \varphi) \cdot \frac{\cos^2 \varphi}{A_Q^2} - \Theta(-\cos \varphi) \cdot \frac{\cos^2 \varphi}{A_N^2} \quad (\text{A11})$$

where Θ is the Heaviside step function. The integral Eq. (A9) becomes

$$\begin{aligned} V_{\text{sub}}(\Delta p_N) &= \frac{4}{3} \left(\frac{1}{A_Q^2} + \frac{1}{A_N^2} \right) \\ &= \frac{4}{3} \Delta p_N \left(\frac{1}{\Delta \tilde{p}_Q} + \frac{1}{\Delta \tilde{p}_N} \right) \end{aligned} \quad (\text{A12})$$

where

$$\Delta \tilde{p}_Q \equiv \frac{9}{a_N^2} (\gamma - 1) \frac{D_Q}{\tau_Q} \frac{\eta_Q}{n_Q} \frac{(g_b \varepsilon_{\text{crit}}^N)^2}{(n_Q / \chi_K^Q)} \frac{1}{\Omega^2}, \quad (\text{A13})$$

$$\Delta \tilde{p}_N \equiv \frac{9}{b_Q^2} (\gamma - 1) \frac{D_N}{\tau_N} \frac{\eta_N}{n_Q} \frac{(g_b \varepsilon_{\text{crit}}^N)^2}{(n_N / \chi_K^N)} \frac{1}{\Omega^2}. \quad (\text{A14})$$

At sufficiently low oscillation amplitude, the integral $V_{\text{sub}}(\Delta p_N)$ is dominated by the term with the smaller value of A . For the class of models we have analyzed, in general $A_Q \gg A_N \gg 1$ ($\Delta \tilde{p}_Q \gg \Delta \tilde{p}_N \gg \Delta p_N$), because in nuclear matter diffusion is less efficient ($D_N/D_Q \approx O(10^{-2})$) and weak interactions take more time to proceed ($\tau_N/\tau_Q \approx O(10^2)$). Therefore the QM \rightarrow NM transition half cycle dominates the dissipation and Eq. (A12) becomes

$$V_{\text{sub}}(\Delta p_N) \xrightarrow{\Delta \tilde{p}_Q \gg \Delta \tilde{p}_N \gg \Delta p_N} \frac{4}{3} \Delta p_N / \Delta \tilde{p}_N. \quad (\text{A15})$$

Performing the angular integral in Eq. (A8) gives the expression for dissipated power $P_{\text{dis}} \equiv W \cdot (\Omega/2\pi)$ at low amplitude

$$P_{\text{dis}}^{\text{sub}}(\alpha) \approx \frac{\alpha^3}{15} \left(\frac{105}{756\pi} \right)^{3/2} \frac{\gamma - 1}{\Delta \tilde{p}_N} \frac{(\varepsilon_{\text{crit}}^N)^2 \Omega^7 \bar{R}_b^{11}}{g_b R^3}. \quad (\text{A16})$$

The power emitted by the mode as gravitational radiation is [49]

$$P_{\text{gr}} \equiv \left(\frac{d\tilde{E}}{dt} \right)_{\text{GR}} = \frac{2^{17} \pi}{3^8 5^2} \alpha^2 G M^2 R^6 \tilde{J}^2 \Omega^8 \quad (\text{A17})$$

The radial integral constant is given by

$$\tilde{J} \equiv \frac{1}{MR^4} \int_0^R \varepsilon(r) r^6 dr \quad (\text{A18})$$

and its typical value for hybrid stars is $\simeq 2 \times 10^{-2}$.

The saturation amplitude α_{sat} is determined by the equation

$$P_{\text{dis}} = \left(\frac{d\tilde{E}}{dt} \right)_{\text{GR}} \quad (\text{A19})$$

Solving Eq. (A19) with Eqs. (A14)-(A18), we obtain the low-amplitude approximation for α_{sat}

$$\alpha_{\text{sat}}^{\text{approx}} = \left(\frac{2^{22} \pi^{9/2}}{3^3 \cdot 5^{5/2}} \right) G \frac{\tilde{D}_N}{\tau_N} \frac{(\chi_K^N)^3}{n_Q n_N^3 b_Q^2} \frac{g_b^3 M^2 \tilde{J}^2}{\Omega} \frac{R^9}{\bar{R}_b^{11}} \quad (\text{A20})$$

where $D_N \equiv \tilde{D}_N \cdot T^{-2}$ (see Eq. (54)).

Appendix B: Range of validity of the analytical approximation for the saturation amplitude

To give an estimate for the validity of the analytic expression for the saturation amplitude, we have to compute Eq. (A11) to NNLO

$$\begin{aligned} s(\varphi) &= \cos^2 \varphi \left[\frac{\Theta(\cos \varphi)}{A_Q^2} - \frac{\Theta(-\cos \varphi)}{A_N^2} \right] \\ &+ (4 \cos^2 \varphi \sin^2 \varphi) \left(\frac{1}{A_Q^4} + \frac{1}{A_N^4} \right) \\ &+ (-8 \cos^4 \varphi + 20 \cos^2 \varphi \sin^2 \varphi) \\ &\times \left[\frac{\Theta(\cos \varphi)}{A_Q^6} - \frac{\Theta(-\cos \varphi)}{A_N^6} \right] + \dots \end{aligned} \quad (\text{B1})$$

in order to obtain the NLO correction to Eq. (A12)

$$\begin{aligned} V_{\text{sub}}(\Delta p_N) &= \frac{4}{3} \left(\frac{1}{A_Q^2} + \frac{1}{A_N^2} \right) \\ &- \frac{16}{5} \left(\frac{1}{A_Q^6} + \frac{1}{A_N^6} \right) + \dots \end{aligned} \quad (\text{B2})$$

This yields the correction term to the dissipated power in the low-amplitude regime

$$P_{\text{dis}}^{\text{sub}}(\alpha) = P_0(\alpha) + P_1(\alpha) + \dots \quad (\text{B3})$$

where P_0 is the previous result Eq. (A16) and the NLO correction reads

$$\begin{aligned} P_1(\alpha) &= -\frac{2\alpha^5}{105} \left(\frac{105}{756\pi} \right)^{5/2} \\ &\times \frac{\gamma - 1}{(\Delta \tilde{p}_N)^3} \frac{(\varepsilon_{\text{crit}}^N)^4 \Omega^{11} \bar{R}_b^{17}}{g_b R^5} \end{aligned} \quad (\text{B4})$$

The requirement that the analytical approximation for the saturation amplitude (Eq. (A20)) deviates from the exact result by less than a fraction ϵ , i.e. $P_1(\alpha_{\text{sat}}^{\text{LO}}) \leq \epsilon P_0(\alpha_{\text{sat}}^{\text{LO}})$ yields the bound on the underlying parameters

$$\frac{2^{39}\pi^5}{3^{12}5^4} \frac{G^2}{(\gamma-1)^2} \frac{g_b M^4 \tilde{J}^4 \Omega^6}{(\varepsilon_{\text{crit}}^{\text{N}})^2} \left(\frac{R}{\bar{R}_b}\right)^{16} \leq \epsilon, \quad (\text{B5})$$

We can see for the set of parameter values on the left-hand side below $\epsilon \ll 1$, Eq. (A20) is a good approximation. With the EoS we applied in Fig. 8, for $\bar{R}_b/R = 0.56$, the left-hand side is ≈ 0.04 ; for $\bar{R}_b/R = (\bar{R}_b/R)_{\text{crit}} = 0.38$ at $\alpha = \alpha_{\text{sat}}^{\text{max}}$, it is ≈ 4 .

Acknowledgments

We thank Mikhail Gusakov for pointing out the chemical potential constraint on front speeds, and Charles Horowitz and Brynmor Haskell for useful discussions. This research was supported in part by the Office of Nuclear Physics of the U.S. Department of Energy under contract #DE-FG02-05ER41375 and by the DOE Topical Collaboration ‘‘Neutrinos and Nucleosynthesis in Hot and Dense Matter’’, contract #DE-SC0004955.

-
- [1] R. F. Sawyer, *Bulk viscosity of hot neutron-star matter and the maximum rotation rates of neutron stars*, Phys. Rev. **D39** (1989) 3804–3806.
- [2] P. Haensel and R. Schaeffer, *Bulk viscosity of hot-neutron-star matter from direct URCA processes*, Phys. Rev. **D45** (1992) 4708–4712.
- [3] J. Madsen, *Bulk viscosity of strange dark matter, damping of quark star vibration, and the maximum rotation rate of pulsars*, Phys. Rev. **D46** (1992) 3290–3295.
- [4] P. Haensel, K. P. Levenfish, and D. G. Yakovlev, *Bulk viscosity in superfluid neutron star cores. I. Direct Urca processes in npe μ matter*, Astron. Astrophys. **357** (2000) 1157–1169, [astro-ph/0004183].
- [5] P. Haensel, K. P. Levenfish, and D. G. Yakovlev, *Bulk viscosity in superfluid neutron star cores. II. Modified Urca processes in npe μ matter*, Astron. Astrophys. **327** (2001) 130–137, [astro-ph/0103290].
- [6] P. Haensel, K. P. Levenfish, and D. G. Yakovlev, *Bulk viscosity in superfluid neutron star cores. III. Effects of Σ^- hyperons*, Astron. Astrophys. **381** (2002) 1080–1089, [astro-ph/0110575].
- [7] P. B. Jones, *Bulk viscosity of neutron-star matter*, Phys. Rev. **D64** (2001) 084003.
- [8] M. G. Alford and A. Schmitt, *Bulk viscosity in 2SC quark matter*, J. Phys. **G34** (2007) 67–102, [nucl-th/0608019].
- [9] C. Manuel and F. J. Llanes-Estrada, *Bulk viscosity in a cold CFL superfluid*, JCAP **0708** (2007) 001, [arXiv:0705.3909].
- [10] M. G. Alford, M. Braby, S. Reddy, and T. Schafer, *Bulk viscosity due to kaons in color-flavor-locked quark matter*, Phys. Rev. **C75** (2007) 055209, [nucl-th/0701067].
- [11] M. Mannarelli and C. Manuel, *Bulk viscosities of a cold relativistic superfluid: color- flavor locked quark matter*, Phys. Rev. **D81** (2010) 043002, [arXiv:0909.4486].
- [12] X. Wang and I. A. Shovkovy, *Bulk viscosity of spin-one color superconducting strange quark matter*, Phys.Rev. **D82** (2010) 085007, [arXiv:1006.1293].
- [13] K. Schwenzer, *How long-range interactions tune the damping in compact stars*, arXiv:1212.5242.
- [14] C. Manuel, J. Tarrus, and L. Tolos, *Bulk viscosity coefficients due to phonons in superfluid neutron stars*, JCAP **1307** (2013) 003, [arXiv:1302.5447].
- [15] L. Lindblom, B. J. Owen, and G. Ushomirsky, *Effect of a neutron star crust on the r mode instability*, Phys.Rev. **D62** (2000) 084030, [astro-ph/0006242].
- [16] J. L. Friedman and B. F. Schutz, *Secular instability of rotating Newtonian stars*, Astrophys. J. **222** (1978) 281.
- [17] N. Andersson, *A new class of unstable modes of rotating relativistic stars*, Astrophys. J. **502** (1998) 708–713, [gr-qc/9706075].
- [18] N. Andersson and K. D. Kokkotas, *The R-mode instability in rotating neutron stars*, Int. J. Mod. Phys. **D10** (2001) 381–442, [gr-qc/0010102].
- [19] L. Lindblom, J. E. Tohline, and M. Vallisneri, *Non-Linear Evolution of the r-Modes in Neutron Stars*, Phys. Rev. Lett. **86** (2001) 1152–1155, [astro-ph/0010653].
- [20] P. Arras et. al., *Saturation of the r-mode instability*, Astrophys. J. **591** (2003) 1129–1151, [astro-ph/0202345].
- [21] R. Bondarescu, S. A. Teukolsky, and I. Wasserman, *Spin Evolution of Accreting Neutron Stars: Nonlinear Development of the R-mode Instability*, Phys. Rev. **D76** (2007) 064019, [arXiv:0704.0799].
- [22] M. G. Alford, S. Mahmoodifar, and K. Schwenzer, *Viscous damping of r-modes: Large amplitude saturation*, Phys.Rev. **D85** (2012) 044051, [arXiv:1103.3521].
- [23] R. Bondarescu and I. Wasserman, *Nonlinear Development of the R-Mode Instability and the Maximum Rotation Rate of Neutron Stars*, Astrophys.J. **778** (2013) 9, [arXiv:1305.2335].
- [24] B. Haskell, K. Glampedakis, and N. Andersson, *A new mechanism for saturating unstable r-modes in neutron stars*, arXiv:1307.0985.
- [25] M. G. Alford, S. Mahmoodifar, and K. Schwenzer, *Large amplitude behavior of the bulk viscosity of dense matter*, J. Phys. **G37** (2010) 125202, [arXiv:1005.3769].
- [26] M. G. Alford, S. Reddy, and K. Schwenzer, *Bridging the Gap by Squeezing Superfluid Matter*, Phys.Rev.Lett. **108** (2012) 111102, [arXiv:1110.6213].
- [27] M. Alford, S. Mahmoodifar, and K. Schwenzer, *Viscous damping of r-modes: Small amplitude instability*, Phys.Rev. **D85** (2012) 024007, [arXiv:1012.4883].
- [28] J. Oppenheimer and G. Volkoff, *On Massive neutron cores*, Phys.Rev. **55** (1939) 374–381.
- [29] J. Horvath and O. Benvenuto, *On the Stability of Slow Neutron Combustion in Astrophysical Objects*, Phys.Lett. **B213** (1988) 516–520.
- [30] A. Drago, A. Lavagno, and I. Parenti, *Burning of an hadronic star into a quark or a hybrid star*, Astrophys.J. **659** (2007) 1519–1535, [astro-ph/0512652].

- [31] M. Herzog and F. K. Ropke, *Three-dimensional hydrodynamic simulations of the combustion of a neutron star into a quark star*, Phys.Rev. **D84** (2011) 083002, [arXiv:1109.0539].
- [32] G. Pagliara, M. Herzog, and F. Ropke, *Combustion of a neutron star into a strange quark star: The neutrino signal*, Phys.Rev. **D87** (2013) 103007, [arXiv:1304.6884].
- [33] A. V. Olinto, *On the Conversion of Neutron Stars Into Strange Stars*, Phys.Lett. **B192** (1987) 71.
- [34] J. Madsen, *Rate of the weak reaction $s + u \rightarrow u + d$ in quark matter*, Phys.Rev. **D47** (1993) 325–330.
- [35] H. Heiselberg and C. J. Pethick, *Transport and relaxation in degenerate quark plasmas*, Phys. Rev. **D48** (1993) 2916–2928.
- [36] J. Schaffner and I. N. Mishustin, *Hyperon rich matter in neutron stars*, Phys.Rev. **C53** (1996) 1416–1429, [nucl-th/9506011].
- [37] P. S. Shternin and D. G. Yakovlev, *Shear viscosity in neutron star cores*, Phys. Rev. **D78** (2008) 063006, [arXiv:0808.2018].
- [38] M. G. Alford, S. Han, and M. Prakash, *Generic conditions for stable hybrid stars*, Phys.Rev. **D88** (2013), no. 8 083013, [arXiv:1302.4732].
- [39] K. Hebeler, J. Lattimer, C. Pethick, and A. Schwenk, *Constraints on neutron star radii based on chiral effective field theory interactions*, Phys.Rev.Lett. **105** (2010) 161102, [arXiv:1007.1746].
- [40] M. G. Alford and K. Schwenzer, *What flashes of pulsars can teach us about their interior*, arXiv:1310.3524.
- [41] S. Mahmoodifar and T. Strohmayer, *Upper bounds on r -mode amplitudes from observations of LMXB neutron stars*, arXiv:1302.1204.
- [42] B. Haskell, N. Degenaar, and W. C. Ho, *Constraining the physics of the r -mode instability in neutron stars with X-ray and UV observations*, Mon.Not.Roy.Astron.Soc. **424** (2012) 93, [arXiv:1201.2101].
- [43] J. Brink, S. A. Teukolsky, and I. Wasserman, *Nonlinear couplings of R -modes: Energy transfer and saturation amplitudes at realistic timescales*, Phys.Rev. **D70** (2004) 121501, [gr-qc/0406085].
- [44] M. G. Alford, A. Schmitt, K. Rajagopal, and T. Schafer, *Color superconductivity in dense quark matter*, Rev. Mod. Phys. **80** (2008) 1455–1515, [arXiv:0709.4635].
- [45] D. G. Ravenhall, C. J. Pethick, and J. R. Wilson, *Structure of matter below nuclear saturation density*, Phys. Rev. Lett. **50** (1983) 2066–2069.
- [46] N. K. Glendenning, *First order phase transitions with more than one conserved charge: Consequences for neutron stars*, Phys. Rev. **D46** (1992) 1274–1287.
- [47] M. G. Alford and G. Good, *Leptonic contribution to the bulk viscosity of nuclear matter*, arXiv:1003.1093.
- [48] B. Niebergal, R. Ouyed, and P. Jaikumar, *Numerical Simulation of the Hydrodynamical Combustion to Strange Quark Matter*, Phys.Rev. **C82** (2010) 062801, [arXiv:1008.4806].
- [49] L. Lindblom, B. J. Owen, and S. M. Morsink, *Gravitational radiation instability in hot young neutron stars*, Phys. Rev. Lett. **80** (1998) 4843–4846, [gr-qc/9803053].
- [50] We thank Mikhail Gusakov for emphasizing this point via personal communications.